Accepted Manuscript

Alu RNA accumulation in hyperglycemia augments oxidative stress and impairs eNOS and SOD2 expression in endothelial cells

Wei Wang, Wei-Hua Wang, Kazem M. Azadzoi, Peng Dai, Qin Wang, Jian-Bin Sun, Wen-Tao Zhang, Yi Shu, Jing-Hua Yang, Zhen Yan

PII: S0303-7207(16)30035-1

DOI: 10.1016/j.mce.2016.02.008

Reference: MCE 9420

To appear in: *Molecular and Cellular Endocrinology*

Received Date: 7 December 2015

Revised Date: 4 February 2016

Accepted Date: 11 February 2016

Please cite this article as: Wang, W., Wang, W.-H., Azadzoi, K.M., Dai, P., Wang, Q., Sun, J.-B., Zhang, W.-T., Shu, Y., Yang, J.-H., Yan, Z., *Alu* RNA accumulation in hyperglycemia augments oxidative stress and impairs eNOS and SOD2 expression in endothelial cells, *Molecular and Cellular Endocrinology* (2016), doi: 10.1016/j.mce.2016.02.008.

Alu RNA accumulation in hyperglycemia augments oxidative stress and impairs eNOS and SOD2 expression in endothelial cells

Wei Wang[a, *], Wei-Hua Wang[a, *], Kazem M. Azadzoi[b], Peng Dai[a], Qin Wang[a], Jian-Bin Sun[a], Wen-Tao Zhang[a], Yi Shu[a], Jing-Hua Yang[a, b, †], Zhen Yan[a, †]

[a] State Key Laboratory of Cancer Biology, Department of Pharmacogenomics, School of Pharmacy, The Fourth Military Medical University, Xi'an 710032, China

[b] Departments of Urology and Surgery, VA Boston Healthcare System, Boston University School of Medicine, Boston 510660, MA, USA

* These authors contributed equally to this work.

[†] Corresponding authors: (yanzhen@fmmu.edu.cn; jyang@bu.edu)

Zhen Yan

State Key Laboratory of Cancer Biology,

Department of Pharmacogenomics,

School of Pharmacy, The Fourth Military Medical University,

Xi'an 710032, China

Tel: +86-29-84772368

E-mail: yanzhen@fmmu.edu.cn

Jinghua Yang

Department of Surgery,

VA Boston Healthcare System, Boston University School of Medicine,

Boston 510660, MA, USA

E-mail: jyang@bu.edu

Abstract

Endothelial dysfunction resulting from oxidative stress and inflammation plays a dominant role in hyperglycemia-induced vasculopathy. While double-stranded RNA (dsRNA) accumulates in redox and inflammatory conditions, its precise role in hyperglycemia-associated endothelial dysfunction remains unclear. This study aimed to investigate whether and how endogenous dsRNA contributes to endothelial dysfunction via oxidative stress. We used a dsRNA-specific antibody J2 to detect and immunoprecipitate cellular dsRNA. Acquired dsRNA was recognized by cDNA library construction and DNA sequencing. Quantitative PCR, ELISA and immunoassays were performed to identify changes induced by acquired dsRNA in primary human umbilical vein endothelial cells (HUVEC). Our data showed that endogenous dsRNA homologous to *Alu* Sc subfamily accumulated in hyperglycemic HUVEC. Comparing *Alu*-transfected HUVEC with high-glucose treated HUVEC, we found that *Alu* RNA elicited the production of reactive oxygen species (ROS) and up-regulated interleukin-1β (IL-1β) expression and secretion in a similar manner as high-glucose treatment. Moreover, *Alu* RNA impeded the expression of endothelial nitric oxide synthase (eNOS) and superoxide dismutase 2 (SOD2), increased ROS production and activated nuclear factor NFκB by chemically scavenging ROS and inactivation of NFκB. The repressed expression of eNOS and SOD2 resulted from *Alu* RNA-mediated negative regulatory mechanisms. Our study uncovered endogenous *Alu* RNA accumulation in hyperglycemic endothelial cells that provoked endothelial oxidative stress and dysfunction by suppressing SOD2 and eNOS expression at both transcription and translation levels via NFκB signaling pathway. These findings suggest a novel regulatory mechanism that involves endogenous dsRNA in endothelial oxidative stress and dysfunction.

Keywords: *Alu* RNA; double-stranded RNA; endothelial cells; Oxidative stress; diabetes

Introduction

Diabetes mellitus is a public health burden as it is increasingly prevalent in both developed and developing countries. Generally, high blood glucose, or hyperglycemia, is the common trait of diabetes. Prolonged exposure to hyperglycemia has been regarded as a key mediator of vascular dysfunction in diabetic patients that will ultimately lead to cardiovascular complications [1]. However, many studies show that vascular endothelium is impaired when blood glucose concentration is below the threshold for the diagnosis of diabetes, suggesting endothelial cell sensitivity to hyperglycemia and endothelial structural modifications in pre-diabetes that lead to progressive vascular dysfunction and cardiovascular complications in the diabetes stage [2]. Therefore, further insight into underlying pathways that initiate endothelial dysfunction and lead to vascular functional deficit is crucial to determining diabetic vascular complications.

Endothelial function is regulated through a dynamic network of nitric oxide (NO) production, reactive oxygen species (ROS) formation and ROS clearance. A causal link in diabetic vasculopathy has been recognized between the NO reduction and the pro-inflammatory / pro-thrombotic state caused by oxidative stress [3]. NO is a key mediator of endothelium-driven smooth muscle relaxation, which is synthesized by NO synthases (NOS) from L-arginine and molecular oxygen [4]. Under hyperglycemic condition, NO is rapidly consumed by reacting with massive superoxide anion (O_2^-) that is produced during the progress of glucose metabolism in endothelial cells with a high rate constant to form peroxynitrite ($ONOO^-$), high levels of which will penetrate across phospholipid membranes and lead to irreversible and noxious nitration of substrates [5]. Meanwhile, hyperglycemia induces nitric oxide synthase (NOS) uncoupling leading to a shift from NO to superoxide anion (O_2^-) production due to impairment of co-factors and NOS substrates. These adverse reactions including peroxynitrite production and NOS uncoupling result in NO deficiency and O_2^- abundance in hyperglycemia [6,7]. To compensate for lack of NO bioavailability and reduce O_2^- -mediated damage, superoxide dismutase (SOD) increases hydrogen peroxide (H_2O_2) levels by dismutation of superoxide anion [8]. However, H_2O_2 accumulation contributes to the formation of highly reactive hydroxyl radical, for which no

physiologic defense exists leading to activation of catalase and glutathione peroxidase for regulation of H_2O_2 levels. Superoxide anion is the primary ROS produced by mitochondria, which is dismutated to H_2O_2 by SOD [9], a process regulated in endothelial cells by SOD1 located in the cytosol, nucleus and inter-membrane space of mitochondria, and SOD2 expressed solely in the mitochondrial matrix [10]. Many studies found that overexpression of SOD would prevent oxidative cellular damage and inhibit the development of diabetic complications [11-13], suggesting that hyperglycemia-induced pathologic alteration impairs the antioxidant defense of SOD in an elusive way. Therefore, the ROS scavenging system also plays an important role maintaining physiologic levels of ROS and preserving endothelial cell function.

In addition to free radical injury, provocation of endothelial damage by interleukin-1β and leukocytes has also been documented [1,14]. In addition to endothelium, cellular ROS is believed to be casually related to inflammation and the expression of inflammatory factors in almost all tissues [15]. The involvement of a class of endogenous dsRNA, *Alu* RNA, in ROS production and inflammation was recently documented, showing that *Alu* RNA accumulation contributes to oxidative stress and degeneration of retinal pigment epithelial cells [16-19]. These findings imply the existence of endogenous dsRNA and its pro-oxidative/ pro-inflammatory roles in the affected tissues. Our goal was to examine endogenous dsRNA expression in hyperglycemic endothelial cells and assess its potential pro-oxidative and pro-inflammatory role in endothelial dysfunction.

Materials and methods

Cells and reagents Human umbilical vein endothelial cells (HUVEC) were collected by collagenase type II treatment of umbilical cord veins as described [20]. This study conforms to the guidelines of the Declaration of Helsinki and was approved by Xijing Hospital Ethics Committee. HUVEC were cultured in M200 medium (Gibco) supplemented with low serum growth supplement (LSGS, Gibco) and 1% penicillin/streptomycin (Hyclone). HUVEC between 3rd to 5th passages were used. M200 medium supplemented with D-glucose up to 25.6 mmol/L was used as the high-glucose medium. After incubated with high-glucose medium for 24 hours, HUVEC were collected for gene expression analysis and western blotting. Transfection reagent jetPEI-HUVEC (Polyplus-transfection Inc.) was used for HUVEC following manufacturer's instruction. Mitochondrial ROS inhibitor ((2-(2,2,6,6-Tetramethylpiperidin-1-oxyl-4-ylamino)-2-oxoethyl) triphenylphosphonium chloride, Mito-TEMPO) and NFκB inhibitor (ammonium pyrrolidinedithiocarbamate, PDTC) were purchased from Sigma Aldrich.

Immunoassays For immunofluorescent assay, cells were seeded on the small coverslips in a 24-well plate. At indicated points, cells were fixed by 4% paraformaldehyde and permeabilized by Triton X-100. Following antibodies were used: anti-factor VIII antibody (1:100, Santa Cruz Biotechnology), J2 antibody (1:200, English & Scientific Consulting, Hungary), FITC labeled anti-mouse /cy3-labeled rabbit IgG (1:1000, Santa Cruz Biotechnology). 4',6-diamidino-2-phenylindole (DAPI, Beyotime Institute of Biotechnology, China) was used to stain the nucleus. Samples were observed under confocal microscope (Olympus FLUOVIEW FV1200). For western blotting, cells were collected at indicated points and lysed by RIPA (CoWin Bioscience, China). Following antibodies were purchased from Santa Cruz Biotechnology and used: anti-NFκB p65 antibody (1:1000), anti-p-NFκB p65 antibody (Ser 536, 1:500), anti-β-actin antibody (1:2000), horse reddish peroxidase (HRP)-conjugated goat anti-mouse / rabbitIgG (1:2000). The immunoblots were detected and quantified using UVP BioImaging System. As for enzyme-linked immunosorbent assay (ELISA), 100μl medium was added in the 96-well plates seeded with HUVEC, and human IL-1β ELISA Set II (BD Biosciences) and human TNF ELISA Set

(BD Biosciences) were used to detect secreted IL-1β and tumor necrosis factor alpha (TNFα) respectively following the manufacturer's instruction.

RNA-immunoprecipitation (RNA-IP) HUVEC were lysed in RIPA (CoWin Bioscience, China) supplemented with protease and phosphatase inhibitors (Roche) and RNase inhibitor (Clontech). The mixture of J2 antibody and protein G agarose (Santa Cruz Biotechnology) was co-incubated with the whole cell lysate overnight at 4℃. After several rinse, dsRNA and J2 antibody was collected by centrifuging and re-suspended in Trizol (Clontech). dsRNA was extracted with chloroform and precipitated by linear acrylamide (Sigmaaldrich), ammonium acetate and isopropanol. Precipitated dsRNA was washed with cold ethanol.

Construction of cDNA library and recombinant plasmids To construct the cDNA library, purified RNA was polyadenylated and reverse transcribed using miRNA First-Strand Synthesis Kit (Clontech). The RNA strand of hybrid cDNA was digested by *E.coli* RNase H, and the second strand cDNA was synthesized by DNA polymerase I and blunted by DNA ligase using cDNA Library Construction Kit (Clontech). An anchor adaptor provided in cDNA Library Construction Kit (Clontech) was ligated to cDNA by T4 DNA ligase and thus the sticky ends were produced. After digestion of the vector with *Eco*R I and *Not* I (Clontech), cDNA was ligated to vector pcDNA3.1(+) (Invitrogen) and transformed into *E*.coli DH5α component cells (Clontech). Clones acquired from the library were sequenced and analyzed. pcDNA3.1(+)-*Alu*-Sc (pAlu) was identified from the library. To produce pAlu-M (G25C; losing the function of impeding translation [21,22]) and pAlu-LA (short-cytoplasmic Alu, left arm only; losing the function of blocking transcription [23]), PCR was performed on pAlu DNA using following primers:
5'-GAATTCGGCCGGGCGCGGTGGCTCACGCCTCTAATC-3' and
5'-CGGCCGTTTTTTTGAGACGGAG-3' for pAlu-M;
5'-GAATTCGGCCGGGCGCGGTGGCTCA-3' and 5'-CGGCCGTTAGTAGAGACGGGGTTTC-3' for pAlu-LA. Amplified DNA were digested by *Eco*R I and *Not* I and then ligated to pcDNA3.1(+). Recombinant plasmids were transformed into *E.coli* DH5α component cells (Clontech) for

amplification, and the inserted fragments were sequenced by Beijing AuGCT DNA-SYN Biotechnology, China.

Dot blotting Equal amounts of total proteins were diluted with 20 × SSC buffer, spotted onto nitrocellulose membrane(Millipore) and fixed at 80°C for 2 hours. After blocking, the membranes were incubated with J2 antibody (1:1,000) for 1 hour. The HRP-conjugated IgG (1:2000) was used for 1 hour. After several washes, the signals were visualized by enhanced chemiluminescence (Millipore).The density of each dot was scanned and quantified by Image-J.

Gene expression analysis Real-time quantitative polymerase chain reaction(qPCR) was performed to check gene expression levels. Total RNA was extracted using RNA Extraction Kit (Clontech) and reverse transcribed using RT reagent kit with gDNA Eraser (Clontech) following the manufacturers' protocol. The reverse transcription products (cDNA) were amplified by qPCR (Applied Biosystems 7500Fast Real-Time PCR system) with SYBR Premix Ex Taq II (Clontech). Following primers were used: NOS2, 5'-CCCACCAGACAGTGCGCCTG-3' and 5'-GGAGCAGCAGCTGGGTTGGG-3'; NOS3, 5'-CCAGCTAGCCAAAGTCACCAT-3' and 5'-GTCTCGGAGCCATACAGGATT-3'; SOD1, 5'-AGCATTAAAGGACTGACTGAAGG-3' and 5'-GTCTCCAACATGCCTCTCTTC-3'; SOD2, 5'-GTTGGGGTTGGCTTGGTTTC-3' and 5'-ATAAGGCCTGTTGTTCCTTGC-3'; CAT, 5'-AGGGGCCTTTGGCTACTTTG-3' and 5'-ACCCGATTCTCCAGCAACAG-3'; TNFα, 5'-CCTCTCTCTAATCAGCCCTCTGG-3' and 5'-TATCTCTCAGCTCCACGCCATT-3'; *Alu*-Sc, 5'-CCTGGCCAACATGGTGAAA-3' and 5'-TCACTGAAACCTCCATCTC-3'; β-actin: 5'-GCTCCTCCTGAGCGCAAG-3' and 5'-CATCTGCTGGAAGGTGGACA-3'. Following PCR, melt curve analysis and agarose gel based quality check were performed to evaluate the quality and specificity of PCR amplifications. For negative controls, none of RT products were added as templates in the qPCR and verified by the absence of gel detected bands. The expression levels of target genes were determined by the $2^{-\Delta\Delta Ct}$ method.

ROS measurement using DCFH-DA fluorescence Dichloro-dihydro-fluorescein diacetate (DCFH-DA, Beyotime Institute of Biotechnology, China) was used to measure the production of ROS. After high-glucose or transfection treatment, cells were washed and incubated with 10 μmol/L DCFH-DA in DMEM for 20min at 37℃. At the end of incubation, wash cells three times to wipe off residual DCFH-DA and then fluorescence microscopy was performed to capture differences between each group.

Statistical analysis Statistical analyses were performed using PASW Statistics 18.0. Differences between means were assessed by Student's *t*-test for two samples, and one-way ANOVA followed by Dunnett's post hoc test for multiple comparisons. All experiments were independently repeated three times and data were shown as mean ± standard error of mean (SEM). Significance was set at a p-value of less than 0.05.

Results

Double-stranded RNA (dsRNA) accumulates in hyperglycemic HUVEC.

Hyperglycemia induced endothelial dysfunction results from oxidative stress and inflammation. Although dsRNA is greatly produced during cell degeneration and inflammatory responses [19,24,25], there is little evidence of the role of dsRNA in endothelial oxidative damage and inflammation under hyperglycemic conditions. To investigate whether dsRNA participates in high-glucose induced vascular injury, we used collagenase type II to collect primary human umbilical vein endothelial cells (HUVEC) and to culture HUVEC *in vitro*. As factor VIII specifically expressed on the plasma and nuclear membranes of endothelial cells, we first identified the characteristics of HUVEC using Cy3-labelled anti-factor VIII antibody and HEK 293T cells was used as a control. By florescent microscopy, it was shown that factor VIII expressed on the endomembrane of endothelial cells (**Fig. S1**).To recognize dsRNA, the specific antibody J2 was employed, which has been successfully used to recognizes dsRNA produced during viral infection, synthesized polyinosinic-polycytidylic acid, endogenous *Alu* RNA, etc. [19,24,26]. Florescent confocal microscopy revealed that under high glucose treatment (25.6mmol/L) for 24 hours, a considerable amount of dsRNA accumulated in the cytoplasm in comparison with euglycemic HUVEC (**Fig. 1 A**). Meanwhile, the whole cell lysate was collected and equal amount of lysate both containing 1μg total proteins were dotted onto the nitrocellulose membrane to quantify dsRNA using J2 antibody. It revealed that dsRNA was produced nearly three folds greater in hyperglycemia versus euglycemia condition (**Fig. 1 B**).

High glucose-induced dsRNA was identified as *Alu*-Sc subfamily.

To determine the nature of dsRNA induced by high glucose, we adopted J2 antibody to immunoprecipitate dsRNA and constructed the complementary DNA (cDNA) library. Thirty-eight clones were obtained from the cDNA library. By DNA sequencing, we found 31 clones (~82%) belonged to *Alu* family and 23 clones (~61%) were highly homologous to *Alu*-Sc subfamily (Fig. 2 A & S2). In consistent with particular structures of *Alu* RNA, dsRNA obtained from hyperglycemic

HUVEC contained the Box A and Box B of RNA polymerase III promoter (**Fig. 2 A, underlined in orange**), the middle A-stretch and the terminal A-stretch (**Fig. 2 A, underlined in green and red**). To quantify the differences between both glycemic conditions, we designed a specific primer pair according to the signature sequence flanking the middle A-stretch of *Alu*-Sc (sequences of primers were shown in Methods). *Alu*-Sc RNA about 250bp was amplified and confirmed by DNA sequencing (**Fig. S3**) and quantitated by quantitative polymerase chain reaction (qPCR). It showed that *Alu*-Sc RNA was increasingly transcribed in hyperglycemic HUVEC (**Fig. 2 B**).

***Alu* RNA promotes the production of reactive oxygen species (ROS) and pro-inflammatory interleukin-1β (IL-1β).**

Prolonged oxidative stress and inflammation are primary inducers of nitric oxide (NO) reduction and inflammatory infiltration [1,4]. In endothelium, excessive ROS augments the expression of pro-inflammatory factors, among which, IL-1β plays a pivotal role in diabetic complications [15]. To investigated the roles of *Alu*-Sc in high-glucose treated HUVEC, pcDNA3.1(+)-*Alu*-Sc (pAlu) obtained from cDNA library was transfected into HUVEC to overexpress *Alu*-Sc RNA in euglycemic HUVEC. To examine superoxide production with high-glucose treatment or with *Alu* RNA overexpression, the ROS specific florescent probe DCFH-DA was loaded into cells in order to label cellular ROS. Comparing with the euglycemic group, high glucose was found to induce ROS and increase its production significantly (**Fig. 3 A**), supporting the concept that hyperglycemia contributes to endothelial dysfunction via oxidative mechanisms. To examine whether *Alu* RNA participated in the process of ROS production, pAlu was transfected into euglycemic HUVEC and pcDNA3.1(+)-Flag (pNull) was used as a non-sense control. It was shown that transfected *Alu*-Sc RNA could induce ROS production as strong as the high glucose treatment (**Fig. 3 B**). Additionally, transfected pAlu was shown as expected to form double-stranded structure that could be recognized by dsRNA-specific J2 antibody under fluorescent microscope (**Fig. S4**), which suggested that *Alu*-Sc RNA exists in cells in a double-stranded form similar to natural *Alu* RNA. Subsequently, the expression and secretion of downstream inflammatory factor, IL-1β, was examined by quantitative PCR and ELISA,

respectively. It was found that IL-1β expression significantly increased in cells (**Fig. 4 A**) and its extracellular secretion was significantly enhanced (**Fig. 4 B**) under high-glucose condition. Surprisingly, pAlu transfection also augmented intracellular expression and extracellular secretion of IL-1β (**Fig. 4 A, B**). To assess the close correlation between IL-1β production and ROS formation, we incubated cultured cells with mitochondria-targeted antioxidant, Mito-TEMPO, at 5 μmol/L for 2 hours following transfection for 24 hours to scavenge ROS [27,28]. Treatment with Mito-TEMPO diminished IL-1β expression and reversed the secretion of IL-1β to the level that was comparable to the control group (**Fig. 4 A, B**). Along with inflammatory infiltration and ROS production, the injury of vasculature is usually correlated with the production of the cytokine tumor necrosis factor-alpha (TNFα), which facilitates glutathione depletion and ROS production via NADPH oxidase and ceramide [29,30]. We thus examined the transcription and secretion of TNFα. As expected, TNFα was significantly increased in mRNA level (**Fig. 4 C**) and in extracellular secretion (**Fig. 4 D**) under high-glucose condition. However, pAlu transfection had little effect on TNFα expression (**Fig. 4 C, D**), which means *Alu* RNA is not involved in TNFα-related signaling. Cumulatively, these data suggest that *Alu* RNA play a crucial role in ROS production in hyperglycemia induced endothelial dysfunction.

***Alu* RNA impedes the expression of NOS and SOD.**

Endothelial dysfunction in hyperglycemia may result from an imbalance between NO bioavailability and ROS production [1,3,9]. Accumulating superoxide anion interacts with NO to produce nitrotyrosin, resulting in diminished NO bioavailability and activation of nitrosative radicals. These processes involve multiple enzymes including eNOS, nNOS and iNOS for NO biosynthesis and SOD1, SOD2 and catalase for superoxide clearage [1,8-10]. To determine whether *Alu* RNA affects NO biosynthesis, we performed the quantitative reverse transcription PCR (qRT-PCR) to analyze relevant gene expressions. With high-glucose stimulation, eNOS expression was decreased (**Fig. 5 B**) while iNOS did not change (**Fig. 5 A**), suggesting eNOS regulation of reduced NO in hyperglycemia. Similarly, *Alu* RNA transfection impaired eNOS expression while having no effect on iNOS (**Fig. 5 A, B**). When Mito-TEMPO was used to

scavenge ROS, *Alu* induced down-regulation of eNOS was prevented (**Fig. 5 B**). These findings imply that *Alu* RNA mediated ROS induced down-regulation of eNOS. To further verify *Alu*-induced impairment of eNOS, western blotting was performed to examine eNOS protein expression. Consistent with qRT-PCR analysis, western blotting confirmed down-regulation of eNOS protein expression with high-glucose stimulation and *Alu* RNA accumulation, and the reduction was also reversed by ROS scavengers (**Fig. 5 C**). We also examined mRNA levels of SOD1/2 and catalase (CAT) as O_2^- is dismutated into H_2O_2 by SOD1/2 and then H_2O_2 is broken down by CAT. We found that while SOD2 and CAT expression diminished significantly (**Fig. 6 B, C**), SOD1 levels decreased but did not meet significance under high–glucose condition (**Fig. 6 A**). In euglycemic HUVEC that were transfected with pAlu, SOD2 transcription decreased and was restored by ROS scavenger (**Fig. 6 B**), while CAT transcription did not change significantly (**Fig. 6 C**). Western blotting revealed that transitional changes in SOD2 expression were consistent with its transcription level (**Fig.6 D**). These findings suggest *Alu* RNA regulation of eNOS and SOD2 expression in the hyperglycemic conditions.

Alu RNA activates NFκB signaling to induce endothelial oxidative stress.

Both oxidative stress and inflammation require the activation of NFκB pathway, which has been implicated in the development of hyperglycemic vasculopathy [3,31,32]. Our goal was to examine the role of *Alu* RNA in NFκB signaling. NFκB is characterized with several isoforms and its activation is mediated by the phosphorylation of p65 subunit [33]. By western blotting, we verified that NFκB p65 was phosphorylated in a time-dependent manner under high-glucose condition (**Fig. 7 A**). Intriguingly, NFκB was also phosphorylated in HUVEC transfected with *Alu* RNA (**Fig. 7 B**). To determine whether *Alu* RNA provoked oxidative stress via NFκB, we utilized a chemical inhibitor, PDTC (100 μmol/L) [34], to block NFκB activation after pAlu transfection for 20 hours (**Fig. 7 B**). In qRT-PCR, we found significant up-regulation of eNOS in cells treated with NFκB blocker (pAlu+PDTC) in comparison with cells only transfected with *Alu* RNA at both transcription (**Fig. 7 C**) and translation levels (**Fig. 7D**); whereas the expression of SOD2, which was also adversely affected by *Alu* RNA, was not restored (**Fig. 7 E, F**). qRT-PCR and ELISA revealed that

cytosolic and secreted IL-1β was declined to the normal levels with suppression of NFκB p65 phosphorylation (**Fig. 7 G, H**). These data implied that *Alu* RNA promoted oxidative stress by decreasing SOD2 levels, impairing eNOS expression and augmenting IL-1β via NFκB signaling pathway.

Alu **RNA represses eNOS and SOD2 transcription and SOD2 translation.**

Alu RNA has been reported to adversely affect cellular processes by impairing translation or blocking transcription [21,23,35,36]. To determine how *Alu* RNA interacts with the relevant enzymes, two mutants were produced. pAlu-M contains a point mutation at G25C that loses the function of impeding translation. pAlu-left arm (pAlu-LA), represents a 3' truncated Alu RNA that is unable to block transcription. Both of the sequences are presented in Figure 8 A. After transfection for 24 hours, HUVEC were collected and qRT-PCR was performed to evaluate the transcription of eNOS and SOD2. We found that pAlu-M repressed the transcription of eNOS and SOD2 as pAlu did, while pAlu-LA was incapable of affecting mRNA transcription of eNOS and SOD2 (**Fig. 8 B, C**). By western blotting, we found that SOD2 expression was restored in HUVEC transfected with both mutants, but the eNOS expression was only restored with pAlu-LA transfection (**Fig.8 D**). These observations imply that eNOS was negatively regulated by *Alu* RNA at transcription level and SOD2 was repressed at both transcription and translation level.

Discussion

Our study showed that hyperglycemia induced endogenous dsRNA accumulation in cytoplasm of HUVEC, which was characterized as the *Alu*-Sc subfamily. We also found that stimulation of *Alu* RNA expression in euglycemic HUVEC caused changes that were consistent with those in hyperglycemic HUVEC, including ROS accumulation, IL-1β up-regulation, eNOS and SOD2 down-regulation, and activation of NFκB. *Alu* induced impairment of eNOS and SOD2 expression was restored by cells treatment with ROS scavengers. Inhibition of NFκB restored *Alu*-induced reduction of eNOS and diminished *Alu*-induced expression of IL-1β but had no significant effect on SOD2. We also verified that *Alu* RNA negatively regulated transcription and translation of relevant enzymes in comparison with its mutants. These observations suggest that *Alu* RNA may expedite endothelial oxidative damage by increasing IL-1β expression and secretion and impairing eNOS and SOD2 expression via NFκB pathway and via repressive mechanisms at the level of transcription and translation in hyperglycemic HUVEC.

dsRNA is considered as a stress and danger signal in mammalian cells, as it provokes innate immune responses that will eventually lead to cellular oxidative stress [37,38]. However, several studies using immunohistochemical staining and molecular analysis detected that dsRNA transiently emerges in the pathological conditions [19,24]. For instance, *Alu* RNA was reported in the pathogenesis of age-related macular degeneration to provoke ROS production and activate inflammasome in retinal pigment epithelium [19]. In consistent with these reports, we found that hyperglycemia stimulates *Alu* RNA production in the endothelium. To our knowledge, this is the first evidence showing dsRNA involvement in a metabolic disorder.

Alu elements, a member of the short interspersed elements (SINE) family of repetitive elements, are disseminated in genome DNA and accounts for 10% of calculated mass of human whole genome [39]. *Alu* RNA, which is transcribed from *Alu* elements, is a family of highly conserved, long non-coding dsRNA in primates. Generally, *Alu* elements are considered to be evolved from a fusion of the 5’ and 3’ ends of 7SL RNA gene [40,41]. Following transcription, *Alu* RNA is fold into

a double-stranded dimer as its secondary structure [42]. Some conserved domains in *Alu* elements are the internal RNA polymerase III promoter site that might be critical to *Alu* amplification, an A-rich region (indicated by Mid A-stretch) separating the two halves of a diverged dimer structure, and a long A-run at the 3' end (indicated by Terminal A-stretch) that may account for its transcription termination [43]. Considering these elements, we characterized the obtained dsRNA in hyperglycemia and identified it as *Alu* RNA (shown in Fig. 2A). However, each part between the conserved domains represents accumulated mutations in the *Alu* element itself [43]. Given that, we designed the obtained *Alu*-Sc specific primers to quantify intracellular *Alu* RNA.

In view of the pro-oxidative and pro-inflammatory nature of dsRNA, we speculated that there may be a correlation between *Alu* RNA accumulation and progressive oxidative stress in the hyperglycemic endothelium. Subsequent analysis revealed that *Alu* RNA accumulation in endothelium promoted ROS production. ROS accumulation in hyperglycemia interferes with NO bioavailability and leads to endothelial redox, oxidative injury and functional deficit [1,44]. We thus examined NOS expression to assess NO biosynthesis and examined SOD and CAT expression to evaluate antioxidant enzymatic mechanisms against ROS. Our data suggested that accumulation of *Alu* RNA reduces both eNOS and SOD2 expression. However, it has not been elucidated how *Alu* RNA contribute to the regulation of gene expression and kinase activation. It has been proposed that *Alu* may act by reducing transcription or interfering with translation initiation [21-23]. The ribonucleoprotein complex, signal recognition particle (SRP), is an adaptor consisting of 7SL RNA and six protein subunit [42]. Assembly of *Alu* RNA to SRP 9/14 ensures the inhibition of translation initiation [21]. The point mutation of G25C in pAlu-M blocks the binding site of *Alu* RNA to SRP9/14 and thus disrupts the inhibition of translation initiation. Moreover, the right arm is found to be essential for *Alu* RNA binding to RNA polymerase II, which results in the repression of transcription [23]. We therefore produced the loss-of-function mutant pAlu-LA by deleting the right arm of *Alu*-Sc RNA. Comparing alterations of eNOS and SOD2 caused by pAlu and its mutants, we concluded that *Alu* RNA repressed the transcription of both enzymes and also inhibited the translation of SOD2. These findings provide mechanistic information as to how Alu RNA increases

ROS production, but the ROS-dependent alterations of enzymes in conjunction with IL-1β induced by *Alu* RNA (shown in Fig. 4, 5 & 6) suggest the involvement of additional downstream pathways in high-glucose induced oxidative stress.

High-glucose stimulus resembled the outcome of NFκB activation in endothelium as both produced changes consistent with the inflammatory nature of endothelial dysfunction [45,46]. The downstream IL-1β is reported to be a pivotal factor in mediating inflammatory injury of endothelial cells in metabolic disorders [15]. Our analysis also implied that *Alu* RNA could facilitate the phosphorylation of NFκB p65 subunit, which may be responsible for the IL-1β production under hyperglycemic condition and *Alu* RNA transfection. Except for IL-1β, TNFα serves a role in ROS production, NFκB activation and inflammatory injury [47]. However, our data showed that *Alu* RNA did not affect the expression of TNFα, suggesting that other molecules that facilitate ROS production and inflammation, such as NADPH oxidases system, remains to be investigated. In addition to the pro-inflammatory property, NFκB also acts as a pleiotropic oxidant sensor to promote SOD2 expression [31,32]. We found that SOD2 was not restored while eNOS was increased with inactivation of NFκB. Our data also suggested that impairment of eNOS expression may be mediated by both oxidative stress and the *trans*-regulation of *Alu* RNA, while the reduction of SOD2 involves mechanisms other than the NFκB associated pathways.

In conclusion, we have shown that endogenous double-stranded *Alu* RNA accumulates in hyperglycemic endothelium, and negatively regulates the expression of eNOS and SOD2, resulting in ROS production, NFκB activation and IL-1β expression. These findings support the existence of endogenous dsRNA in endothelium, and suggest the novel *Alu* RNA machinery regulating endothelial oxidative stress and dysfunction.

Acknowledgment

We are grateful to Dr. Meng Li and Ms. Tiannan Jiang for technical assistance with endothelial cell culture. This work was supported by grants from National Natural Science Foundation of China

(81071369, 30928031,81200055 and 31471322), State Project for Essential Drug Research and Development (2009ZX09301-009-BD23), China Postdoctoral Science Foundation (2012M521866) and Grant BLR&D MERIT 1I01BX001428 from the U.S. No potential conflicts of interest were disclosed.

References:

[1] Paneni, F., Beckman, J.A., Creager, M.A. and Cosentino, F. (2013) Diabetes and vascular disease: pathophysiology, clinical consequences, and medical therapy: part I. EUR HEART J 34, 2436-2443.

[2] Rutter, M.K. and Nesto, R.W. (2011) Blood pressure, lipids and glucose in type 2 diabetes: how low should we go? Re-discovering personalized care. EUR HEART J 32, 2247-U132.

[3] Rask-Madsen, C. and King, G.L. (2013) Vascular Complications of Diabetes: Mechanisms of Injury and Protective Factors. CELL METAB 17, 20-33.

[4] Thomas, D.D., Ridnour, L.A., Isenberg, J.S., Flores-Santana, W., Switzer, C.H., Donzelli, S., Hussain, P., Vecoli, C., Paolocci, N., Ambs, S., Colton, C.A., Harris, C.C., Roberts, D.D. and Wink, D.A. (2008) The chemical biology of nitric oxide: implications in cellular signaling. Free Radic Biol Med 45, 18-31.

[5] Kohr, M.J., Roof, S.R., Zweier, J.L. and Ziolo, M.T. (2012) Modulation of myocardial contraction by peroxynitrite. Front Physiol 3, 468.

[6] Tousoulis, D., Antoniades, C., Tentolouris, C., Goumas, G., Stefanadis, C. and Toutouzas, P. (2002) L-arginine in cardiovascular disease: dream or reality? VASC MED 7, 203-11.

[7] Ido, Y., Carling, D. and Ruderman, N. (2002) Hyperglycemia-Induced Apoptosis in Human Umbilical Vein Endothelial Cells. DIABETES 51, 159.

[8] Thomas, S.R., Chen, K. and Keaney, J.J. (2002) Hydrogen peroxide activates endothelial nitric-oxide synthase through coordinated phosphorylation and dephosphorylation via a phosphoinositide 3-kinase-dependent signaling pathway. J BIOL CHEM 277, 6017-24.

[9] Zhang, D.X. and Gutterman, D.D. (2007) Mitochondrial reactive oxygen species-mediated signaling in endothelial cells. American Journal of Physiology - Heart and Circulatory Physiology 292, H2023-H2031.

[10] Okado-Matsumoto, A. and Fridovich, I. (2001) Subcellular distribution of superoxide dismutases (SOD) in rat liver: Cu,Zn-SOD in mitochondria. J BIOL CHEM 276, 38388-93.

[11] Du, Y., Miller, C.M. and Kern, T.S. (2003) Hyperglycemia increases mitochondrial superoxide in retina and retinal cells. FREE RADICAL BIO MED 35, 1491-1499.

[12] Kowluru, R.A., Kowluru, V., Xiong, Y. and Ho, Y. (2006) Overexpression of mitochondrial superoxide dismutase in mice protects the retina from diabetes-induced oxidative stress. FREE RADICAL BIO MED 41, 1191-1196.

[13] Craven, P.A., Melhem, M.F., Phillips, S.L. and DeRubertis, F.R. (2001) Overexpression of Cu2+/Zn2+ superoxide dismutase protects against early diabetic glomerular injury in transgenic mice. DIABETES 50, 2114-25.

[14] Morigi, M., Angioletti, S., Imberti, B., Donadelli, R., Micheletti, G., Figliuzzi, M., Remuzzi, A., Zoja, C. and Remuzzi, G. (1998) Leukocyte-endothelial interaction is augmented by high glucose concentrations and hyperglycemia in a NF-kB-dependent fashion. J CLIN INVEST 101, 1905-15.

[15] Schroder, K., Zhou, R. and Tschopp, J. (2010) The NLRP3 Inflammasome: A Sensor for Metabolic Danger? SCIENCE 327, 296-300.

[16] Kaneko, H., Dridi, S., Tarallo, V., Gelfand, B.D., Fowler, B.J., Cho, W.G., Kleinman, M.E., Ponicsan, S.L.,

Hauswirth, W.W., Chiodo, V.A., Karikó, K., Yoo, J.W., Lee, D., Hadziahmetovic, M., Song, Y., Misra, S., Chaudhuri, G., Buaas, F.W., Braun, R.E., Hinton, D.R., Zhang, Q., Grossniklaus, H.E., Provis, J.M., Madigan, M.C., Milam, A.H., Justice, N.L., Albuquerque, R.J.C., Blandford, A.D., Bogdanovich, S., Hirano, Y., Witta, J., Fuchs, E., Littman, D.R., Ambati, B.K., Rudin, C.M., Chong, M.M.W., Provost, P., Kugel, J.F., Goodrich, J.A., Dunaief, J.L., Baffi, J.Z. and Ambati, J. (2011) DICER1 deficit induces Alu RNA toxicity in age-related macular degeneration. NATURE 471, 325-330.

[17] Gelfand, B.D., Wright, C.B., Kim, Y., Yasuma, T., Yasuma, R., Li, S., Fowler, B.J., Bastos-Carvalho, A., Kerur, N., Uittenbogaard, A., Han, Y.S., Lou, D., Kleinman, M.E., McDonald, W.H., Nunez, G., Georgel, P., Dunaief, J.L. and Ambati, J. (2015) Iron Toxicity in the Retina Requires Alu RNA and the NLRP3 Inflammasome. CELL REP 11, 1686-93.

[18] Kerur, N., Hirano, Y., Tarallo, V., Fowler, B.J., Bastos-Carvalho, A., Yasuma, T., Yasuma, R., Kim, Y., Hinton, D.R., Kirschning, C.J., Gelfand, B.D. and Ambati, J. (2013) TLR-independent and P2X7-dependent signaling mediate Alu RNA-induced NLRP3 inflammasome activation in geographic atrophy. Invest Ophthalmol Vis Sci 54, 7395-401.

[19] Tarallo, V., Hirano, Y., Gelfand, B.D., Dridi, S., Kerur, N., Kim, Y., Cho, W.G., Kaneko, H., Fowler, B.J., Bogdanovich, S., Albuquerque, R.J.C., Hauswirth, W.W., Chiodo, V.A., Kugel, J.F., Goodrich, J.A., Ponicsan, S.L., Chaudhuri, G., Murphy, M.P., Dunaief, J.L., Ambati, B.K., Ogura, Y., Yoo, J.W., Lee, D., Provost, P., Hinton, D.R., Núñez, G., Baffi, J.Z., Kleinman, M.E. and Ambati, J. (2012) DICER1 Loss and Alu RNA Induce Age-Related Macular Degeneration via the NLRP3 Inflammasome and MyD88. CELL 149, 847-859.

[20] Jaffe, E., Nachman, R., Becker, C., Minick, C., Jaffe, E., Nachman, R., Becker, C. and Minick, C. (1973) Culture of human endothelial cells derived from umbilical veins. J CLIN INVEST 52, 2745-2756.

[21] Ivanova, E., Berger, A., Scherrer, A., Alkalaeva, E. and Strub, K. (2015) Alu RNA regulates the cellular pool of active ribosomes by targeted delivery of SRP9/14 to 40S subunits. NUCLEIC ACIDS RES 43, 2874-87.

[22] H Sler, J. and K, S. (2006) Alu RNP and Alu RNA regulate translation initiation in vitro. NUCLEIC ACIDS RES 34, 2374-2385.

[23] Mariner, P.D., Walters, R.D., Espinoza, C.A., Drullinger, L.F., Wagner, S.D., Kugel, J.F. and Goodrich, J.A. (2008) Human Alu RNA is a modular transacting repressor of mRNA transcription during heat shock. MOL CELL 29, 499-509.

[24] Weber, F., Wagner, V., Rasmussen, S.B., Hartmann, R. and Paludan, S.R. (2006) Double-Stranded RNA Is Produced by Positive-Strand RNA Viruses and DNA Viruses but Not in Detectable Amounts by Negative-Strand RNA Viruses. J VIROL 80, 5059-5064.

[25] Chu, W.M., Ballard, R., Carpick, B.W., Williams, B.R. and Schmid, C.W. (1998) Potential Alu function: regulation of the activity of double-stranded RNA-activated kinase PKR. MOL CELL BIOL 18, 58-68.

[26] Bonin, M., Oberstrass, J., Lukacs, N., Ewert, K., Oesterschulze, E., Kassing, R. and Nellen, W. (2000) Determination of preferential binding sites for anti-dsRNA antibodies on double-stranded RNA by scanning force microscopy. RNA 6, 563-70.

[27] Liu, M., Liu, H. and Dudley, S.J. (2010) Reactive oxygen species originating from mitochondria regulate the cardiac sodium channel. CIRC RES 107, 967-74.

[28] Liang, H.L., Sedlic, F., Bosnjak, Z. and Nilakantan, V. (2010) SOD1 and MitoTEMPO partially prevent mitochondrial permeability transition pore opening, necrosis, and mitochondrial apoptosis after ATP depletion recovery. Free Radic Biol Med 49, 1550-60.

[29] Bourraindeloup, M., Adamy, C., Candiani, G., Cailleret, M., Bourin, M.C., Badoual, T., Su, J.B., Adubeiro, S.,

Roudot-Thoraval, F., Dubois-Rande, J.L., Hittinger, L. and Pecker, F. (2004) N-acetylcysteine treatment normalizes serum tumor necrosis factor-alpha level and hinders the progression of cardiac injury in hypertensive rats. CIRCULATION 110, 2003-9.

[30] Su, J.B. (2015) Vascular endothelial dysfunction and pharmacological treatment. World J Cardiol 7, 719-41.

[31] Hamid, C., Norgate, K., D'Cruz, D.P., Khamashta, M.A., Arno, M., Pearson, J.D., Frampton, G. and Murphy, J.J. (2007) Anti-beta2GPI-antibody-induced endothelial cell gene expression profiling reveals induction of novel pro-inflammatory genes potentially involved in primary antiphospholipid syndrome. ANN RHEUM DIS 66, 1000-7.

[32] Kiningham, K.K., Xu, Y., Daosukho, C., Popova, B. and St, C.D. (2001) Nuclear factor kappaB-dependent mechanisms coordinate the synergistic effect of PMA and cytokines on the induction of superoxide dismutase 2. BIOCHEM J 353, 147-156.

[33] Sen, R. and Smale, S.T. (2010) Selectivity of the NF- κ B Response. CSH PERSPECT BIOL 2, a000257-a000257.

[34] DangLi, R., HeKong, W., JiQin, L., MingHua, Z. and WenCheng, Z. (2012) ROS-induced ZNF580 expression: a key role for H2O2/NF-kappaB signaling pathway in vascular endothelial inflammation. MOL CELL BIOCHEM 359, 183-91.

[35] Bennett, E.A., Keller, H., Mills, R.E., Schmidt, S., Moran, J.V., Weichenrieder, O. and Devine, S.E. (2008) Active Alu retrotransposons in the human genome. GENOME RES 18, 1875-1883.

[36] Hasler, J. and Strub, K. (2006) Alu elements as regulators of gene expression. NUCLEIC ACIDS RES 34, 5491-7.

[37] Kumar, M. and Carmichael, G.G. (1998) Antisense RNA: function and fate of duplex RNA in cells of higher eukaryotes. Microbiol Mol Biol Rev 62, 1415-34.

[38] Loo, Y. and Gale, M. (2011) Immune Signaling by RIG-I-like Receptors. IMMUNITY 34, 680-692.

[39] Quentin, Y. (1992) Origin of the Alu family: a family of Alu-like monomers gave birth to the left and the right arms of the Alu elements. NUCLEIC ACIDS RES 20, 3397-401.

[40] Hasler, J. and Strub, K. (2006) Alu elements as regulators of gene expression. NUCLEIC ACIDS RES 34, 5491-5497.

[41] Grover, D., Mukerji, M., Bhatnagar, P., Kannan, K. and Brahmachari, S.K. (2004) Alu repeat analysis in the complete human genome: trends and variations with respect to genomic composition. Bioinformatics (Oxford, England) 20, 813-7.

[42] Hasler, J. and Strub, K. (2006) Alu RNP and Alu RNA regulate translation initiation in vitro. NUCLEIC ACIDS RES 34, 2374-85.

[43] Deininger, P. (2011) Alu elements: know the SINEs. GENOME BIOL 12, 236.

[44] Giacco, F. and Brownlee, M. (2010) Oxidative Stress and Diabetic Complications. CIRC RES 107, 1058-1070.

[45] Brand, K., Page, S., Rogler, G., Bartsch, A., Brandl, R., Knuechel, R., Page, M., Kaltschmidt, C., Baeuerle, P.A. and Neumeier, D. (1996) Activated transcription factor nuclear factor-kappa B is present in the atherosclerotic lesion. J CLIN INVEST 97, 1715-22.

[46] Hong, B., Agranoff, A.B., Leung, K., Neish, A.S., Collins, T. and Nabel, G.J. (1993) Differential regulation of vascular cell adhesion molecule 1 gene expression by specific NF- κ B subunits in endothelial and epithelial cells. Molecular & Cellular Biology 13, 6283-6289.

[47] Brandes, R.P. (2003) Role of NADPH oxidases in the control of vascular gene expression. Antioxid Redox Signal 5, 803-11.

Figure legends

Figure 1. Double-stranded RNA was increasingly expressed in high-glucose treated HUVEC.

(**A**) dsRNA expression by immunofluorescent microscopy. HUVEC cultured in low-glucose (LG) M200 medium (5.6 mmol/L D-glucose) or high-glucose (HG) M200 medium (25.6 mmol/L D-glucose) for 24 hours were fixed and labeled by FITC-labeled J2 antibody (1:200). Micrographs were taken to show dsRNA (green) and nucleus (blue, stained by DAPI) (**B**) dsRNA quantification by dot blotting. Equivalent whole cell lysates of LG and HG treated HUVEC were dotted on nitrocellulose membrane and hybridized with J2 antibody (1:1000). The immune-dot density was scanned by Image-J and shown as the change fold. HG group vs. LG group, ** $P < 0.01$. Data were means ± SEM.

Figure 2. Alu-Sc RNA was identified and increasingly transcribed in high-glucose treated HUVEC.

(**A**) *Alu* RNA sequence alignment. *Alu* RNA contains several conserved sequences: RNase polymerase III binding site (including Box A and Box B, R representing purine, Y representing pyrimidine, N representing any base), mid-A stretch and terminal-A stretch. dsRNA immunoprecipitated from HG-treated HUVEC was cloned, sequenced and aligned with Alu-Sc consensus (Accession:U14571). Conserved sequences were underlined with relevant color. (**B**) *Alu*-Sc transcription level. LG or HG treated HUVEC were collected and total RNA were extracted. qRT-PCR was performed to quantify *Alu*-Sc RNA expression using specific *Alu*-Sc RNA primers. HG group vs. LG group, ** $P < 0.01$. Data were means ± SEM.

Figure 3. *Alu* RNA promoted the production of ROS.

DCFH-DA labeling ROS in (**A**) HG / LG treated HUVEC and in (**B**) pNull / pAlu transfected HUVEC. The rate of fluorescent cells in total cells was counted by Image-J. FL represents florescent field; BF represents bright field. HG group vs. LG group, ** $P < 0.01$. Data were means ± SEM.

Figure 4. *Alu* RNA promoted the expression and secretion of IL-1β.

(**A**) Gene expression of IL-1β was measured in LG /HG treated and pNull / pAlu transfected / Mito-TEMPO (MT, 5 μmol/L) + pAlu treated HUVEC respectively. Fold changes were calculated by $2^{-\Delta\Delta Ct}$ method using β-actin as housekeeping gene. HG group vs. LG group, ***P* < 0.01; pAlu vs. pNull, pAlu+MT vs. pAlu, **P* < 0.05; pAlu+MT vs. pNull, *n.s.* (nonsense) *P* > 0.05. Data were means ± SEM. (**B**) ELISA assay of IL-1β in supernatant of cultured HUVEC. HG group vs. LG group, pAlu / pAlu+MT vs. pNull, ***P* < 0.01. Data were means ± SEM. (**C**) Gene expression of TNFα was measured as described above. HG group vs. LG group, ***P* < 0.01; pAlu vs. pNull, **P* < 0.05; pAlu+MT vs. pAlu, *n.s. P* > 0.05. Data were means ± SEM. (**D**) ELISA assay of TNFα in supernatant of cultured HUVEC. HG group vs. LG group, ***P* < 0.01; one-way ANOVA for comparision among pNull, pAlu and pAlu+MT, *n.s. P* > 0.05. Data were means ± SEM.

Figure 5. *Alu* RNA impaired the expression of eNOS rather than iNOS in a ROS dependent manner.

(**A**, **B**) Gene expression of (**A**) iNOS and (**B**) eNOS was measured in LG /HG treated and pNull / pAlu transfected / Mito-TEMPO (MT) + pAlu treated HUVEC. Fold changes were calculated by $2^{-\Delta\Delta Ct}$ method using β-actin as housekeeping gene. HG group vs. LG group, pAlu vs. pNull, pAlu+MT vs. pAlu, **P* < 0.05, ***P* < 0.01, *n.s. P* > 0.05. Data were means ± SEM. (**C**) eNOS expression was examined by western blotting using anti-eNOS antibody (1:500) and quantified by UVP BioImaging System. The expression level of β-actin was used as the internal control. HG group vs. LG group, pAlu vs. pNull ***P* < 0.01; pAlu+MT vs. pAlu, **P* < 0.05. Data were means ± SEM.

Figure 6. *Alu* RNA impaired the expression of SOD2 in a ROS dependent manner instead of SOD1 and CAT.

(**A**, **B** and **C**) Gene expression of (**A**) SOD1, (**B**) SOD2 and (**C**) CAT was measured in LG /HG treated and pNull / pAlu transfected / Mito-TEMPO (MT) + pAlu treated HUVEC. Fold changes

were calculated by $2^{-\Delta\Delta Ct}$ method using β-actin as housekeeping gene. HG group vs. LG group, pAlu vs. pNull, pAlu+MT vs. pAlu, *P < 0.05, **P < 0.01, *n.s.* P > 0.05. Data were means ± SEM. (**D**) SOD2 expression was examined by western blotting using anti-SOD2 antibody (1:500) and quantified by UVP BioImaging System. The expression level of β-actin was used as the internal control. HG group vs. LG group, pAlu vs. pNull, pAlu+MT vs. pAlu, **P < 0.01. Data were means ± SEM.

Figure 7. *Alu* RNA affected the expression of eNOS and IL-1β via NFκB signal pathway. (**A**) HUVEC were seeded in a 6-well plate, and lysed by RIPA after high glucose treatment for 0, 8, 16, 24, 32 hours respectively. Western blotting was performed to detect phosphor-NFκB p65 subunit (p-NFκB p65, 1:500), NFκB p65 subunit (1:1000), and β-actin (1:2000). Immunoblots were quantified by UVP BioImaging System. Comparing with 0 hour group, **P < 0.01. Data were means ± SEM. (**B**) HUVEC were seeded in a 6-well plates and transfected with pAlu. PDTC (100 μmol/L) was added after transfection for 20 hours. Western blotting was performed to detect NFκB p65 and phosphor-NFκB p65. Immunoblots were quantified by UVP BioImaging System. pAlu vs. pNull, pAlu+PDTC vs. pAlu, **P < 0.01. Data were means ± SEM. (**C**, **E**, and **G**) Gene expression of (**C**) eNOS, (**E**) SOD2 and (**G**) IL-1β were measured in pNull / pAlu transfected / pAlu + P (PDTC) treated HUVEC. Fold changes were calculated by $2^{-\Delta\Delta Ct}$ method using β-actin as housekeeping gene. pAlu vs. pNull, pAlu+P vs. pAlu, **P < 0.01, *n.s.* P > 0.05. Data were means ± SEM. (**D**, **F**) Relevant protein expression of eNOS and SOD2 was measured by western blotting and quantified by UVP BioImaging System. β-actin was used as the internal control. pAlu vs. pNull, pAlu+P vs. pAlu, *P < 0.05, **P < 0.01, *n.s.* P > 0.05. Data were means ± SEM. (**H**) ELISA assay of IL-1β in supernatant of cultured HUVEC. pNull vs.pAlu, pAlu vs. pAlu+P, **P < 0.01. Data were means ± SEM.

Figure 8. *Alu* RNA negatively regulated gene expression in hyperglycemic HUVEC. (**A**) Mutants of pAlu. pAlu-M was point mutation at Alu-Sc G25C (losing the function of impeding

translation). pAlu-LA was a 3' truncated mutation of Alu-Sc 1-120 (losing the function of blocking transcription). (**B, C**) Gene expression of (**B**) eNOS and (**C**) SOD2 was measured in pAlu or the mutants transfected HUVEC. Fold changes were calculated by $2^{-\Delta\Delta Ct}$ method using β-actin as housekeeping gene. pAlu vs. pAlu-M, pAlu vs. Alu-LA, $*P < 0.05$, $**P < 0.01$, *n.s.* $P > 0.05$. Data were means ± SEM. (**D**) Translation levels of eNOS and SOD2 in pAlu and its mutants transfected HUVEC were examined by western blotting and immunoblots were quantified by UVP BioImaging System. β-actin was used as the internal control. Comparing with pAlu, $**P < 0.01$. Data were means ± SEM.

Supplemental Materials

Figure S1. The endothelial cells character identification by using anti-factor VIII antibody on cultured HUVEC. HUVEC were seeded on cover slips, and fixed and permeabilized at ~80% confluence. HEK293T cells were used as a control cell line. Factor VIII was detected by Cy3 (red)-labeled anti-Factor VIII antibody. The box showed Factor VIII dying on plasma and nuclear membranes.

Figure S2. Alignment of Alu DNA sequences obtained from cDNA library.

Figure S3. Agarose gel electrophoresis for the products of *Alu*-Sc RNA amplification using Sc subfamily-specific primers. HUVEC were collected after high / normal-glucose treatment for 24 hours and total RNA was extracted and reverse transcribed. PCR was performed to detect *Alu*-Sc cDNA.

Figure S4. dsRNA detection in pAlu transfected HUVEC. pAlu was transfected into HUVEC that were seeded on cover slips using jetPEI-HUVEC for 24h. Cells were fixed and permeabilized. dsRNA was detected using J2 antibody (1:200). HUVEC transfected by pNull was used as a control.

Figure 1

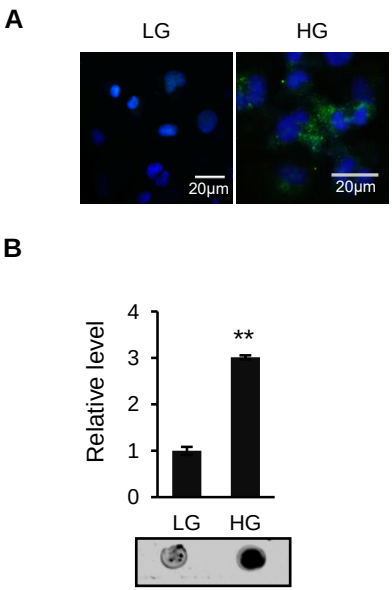

Figure 2

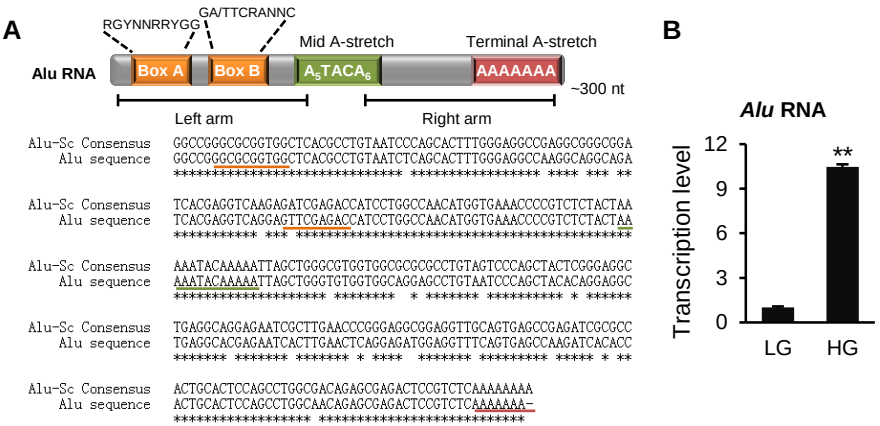
A
RGYNNRRYGG
GA/TTCRANNC
Mid A-stretch
Terminal A-stretch
Alu RNA
Box A
Box B
A5TACA6
AAAAAAA
~300 nt
Left arm
Right arm
Alu-Sc Consensus GGCCGGGCGCGGTGGCTCACGCCTGTAATCCCAGCACTTTGGGAGGCCGAGGCGGGCGGA
Alu sequence GGCCGGGCGCGGTGGCTCACGCCTGTAATCTCAGCACTTTGGGAGGCCAAGGCAGGCAGA
Alu-Sc Consensus TCACGAGGTCAAGAGATCGAGACCATCCTGGCCAACATGGTGAAACCCCGTCTCTACTAA
Alu sequence TCACGAGGTCAGGAGTTCGAGACCATCCTGGCCAACATGGTGAAACCCCGTCTCTACTAA
Alu-Sc Consensus AAATACAAAAATTAGCTGGGCGTGGTGGCGCGCGCCTGTAGTCCCAGCTACTCGGGAGGC
Alu sequence AAATACAAAAATTAGCTGGGTGTGGTGGCAGGAGCCTGTAATCCCAGCTACACAGGAGGC
Alu-Sc Consensus TGAGGCAGGAGAATCGCTTGAACCCGGGAGGCGGAGGTTGCAGTGAGCCGAGATCGCGCC
Alu sequence TGAGGCACGAGAATCACTTGAACTCAGGAGATGGAGGTTTCAGTGAGCCAAGATCACACC
Alu-Sc Consensus ACTGCACTCCAGCCTGGCGACAGAGCGAGACTCCGTCTCAAAAAAAA
Alu sequence ACTGCACTCCAGCCTGGCAACAGAGCGAGACTCCGTCTCAAAAAAA-
B
Alu RNA
Transcription level
12
9
6
3
0
**
LG
HG

Figure 3

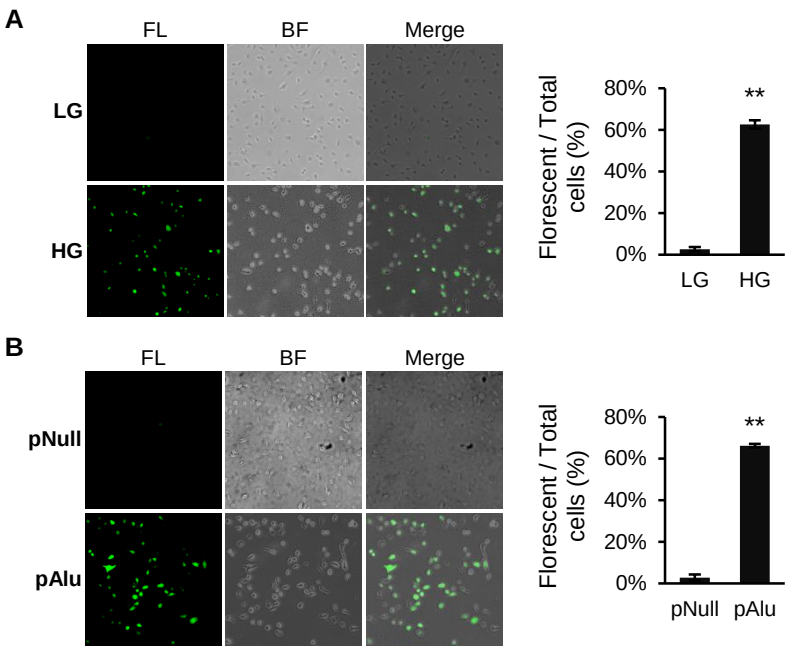
A
FL
BF
Merge
LG
HG
Florescent / Total cells (%)
80%
60%
40%
20%
0%
**
LG
HG
B
FL
BF
Merge
pNull
pAlu
Florescent / Total cells (%)
80%
60%
40%
20%
0%
**
pNull
pAlu

Figure 4

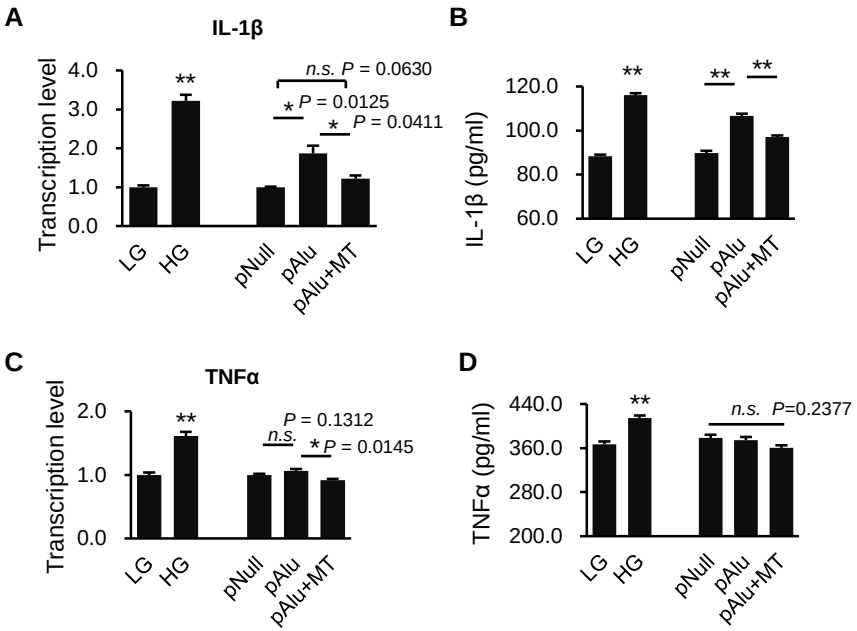
A
IL-1β
Transcription level
4.0
3.0
2.0
1.0
0.0
**
n.s. P = 0.0630
* P = 0.0125
* P = 0.0411
LG
HG
pNull
pAlu
pAlu+MT
B
IL-1β (pg/ml)
120.0
100.0
80.0
60.0
**
**
**
C
TNFα
Transcription level
2.0
1.0
0.0
**
P = 0.1312
n.s.
* P = 0.0145
D
TNFα (pg/ml)
440.0
360.0
280.0
200.0
**
n.s. P=0.2377

Figure 5

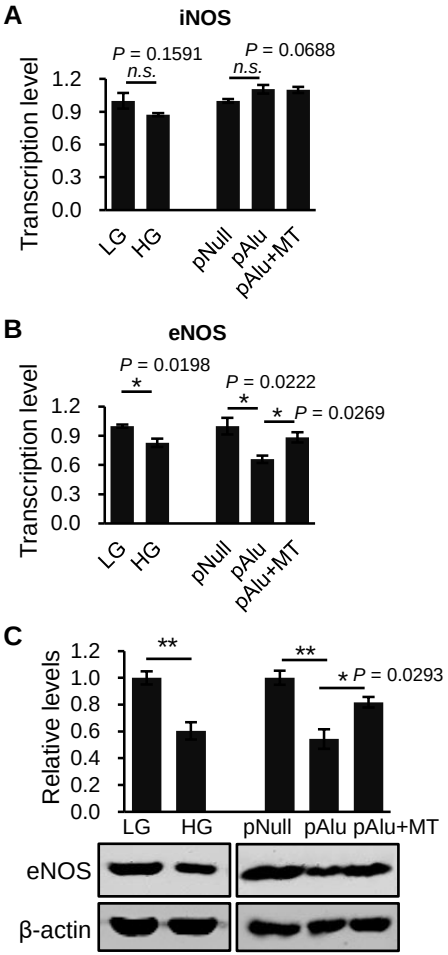
A
iNOS
P = 0.1591
n.s.
P = 0.0688
n.s.
Transcription level
1.2
0.9
0.6
0.3
0.0
LG
HG
pNull
pAlu
pAlu+MT
B
eNOS
P = 0.0198
*
P = 0.0222
*
* P = 0.0269
Transcription level
1.2
0.9
0.6
0.3
0.0
LG
HG
pNull
pAlu
pAlu+MT
C
**
**
* P = 0.0293
Relative levels
1.2
1.0
0.8
0.6
0.4
0.2
0.0
LG
HG
pNull
pAlu
pAlu+MT
eNOS
β-actin

Figure 6

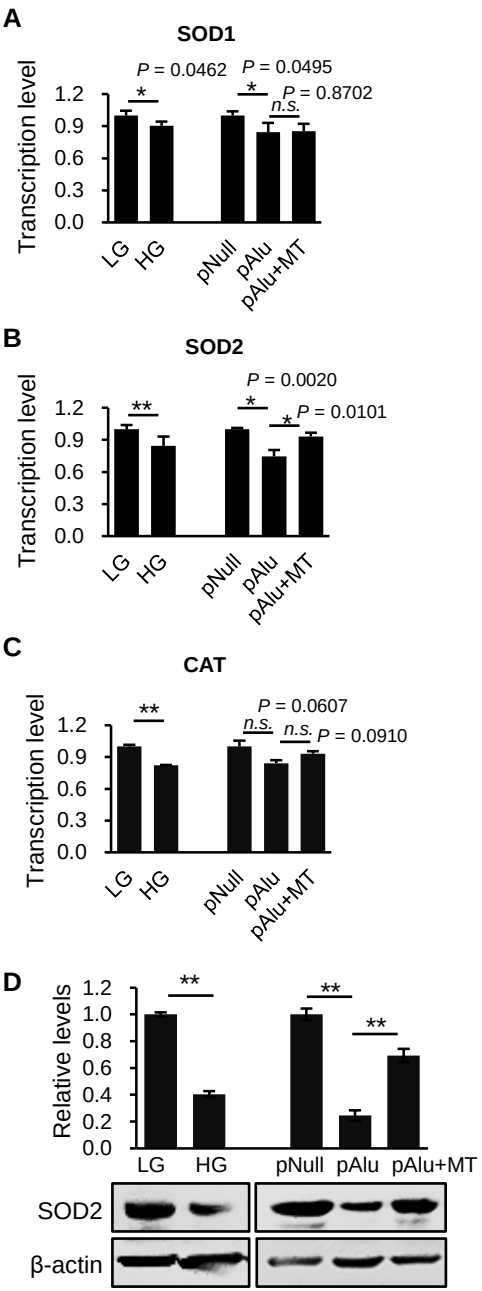
A
SOD1
P = 0.0462
P = 0.0495
P = 0.8702
n.s.
Transcription level
1.2
0.9
0.6
0.3
0.0
LG
HG
pNull
pAlu
pAlu+MT
B
SOD2
P = 0.0020
P = 0.0101
Transcription level
C
CAT
P = 0.0607
n.s.
P = 0.0910
D
Relative levels
1.2
1.0
0.8
0.6
0.4
0.2
0.0
SOD2
β-actin

Figure 7

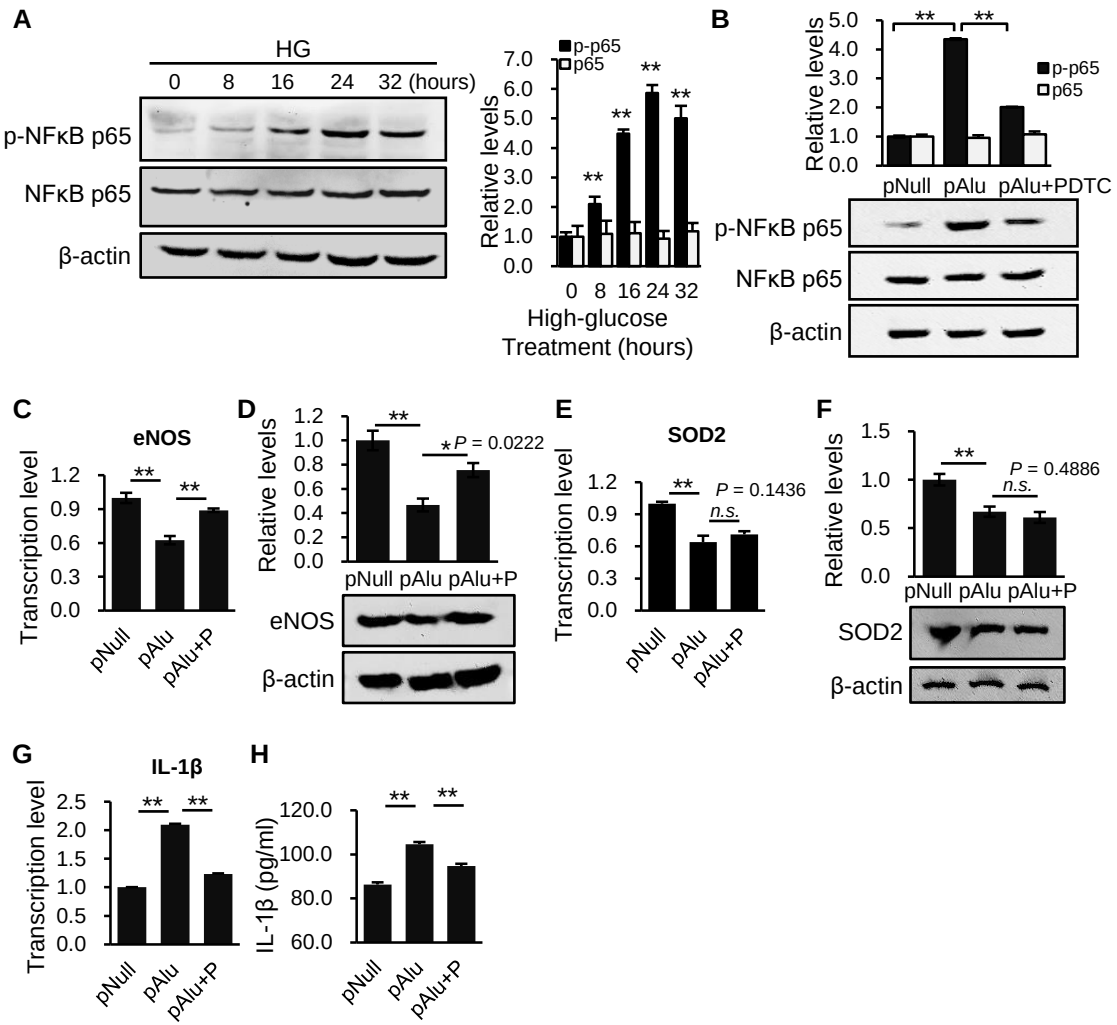
A
HG
0 8 16 24 32 (hours)
p-NFκB p65
NFκB p65
β-actin
p-p65
p65
Relative levels
High-glucose
Treatment (hours)
B
pNull pAlu pAlu+PDTC
C
eNOS
Transcription level
D
P = 0.0222
E
SOD2
P = 0.1436
n.s.
F
P = 0.4886
G
IL-1β
H
IL-1β (pg/ml)

Figure 8

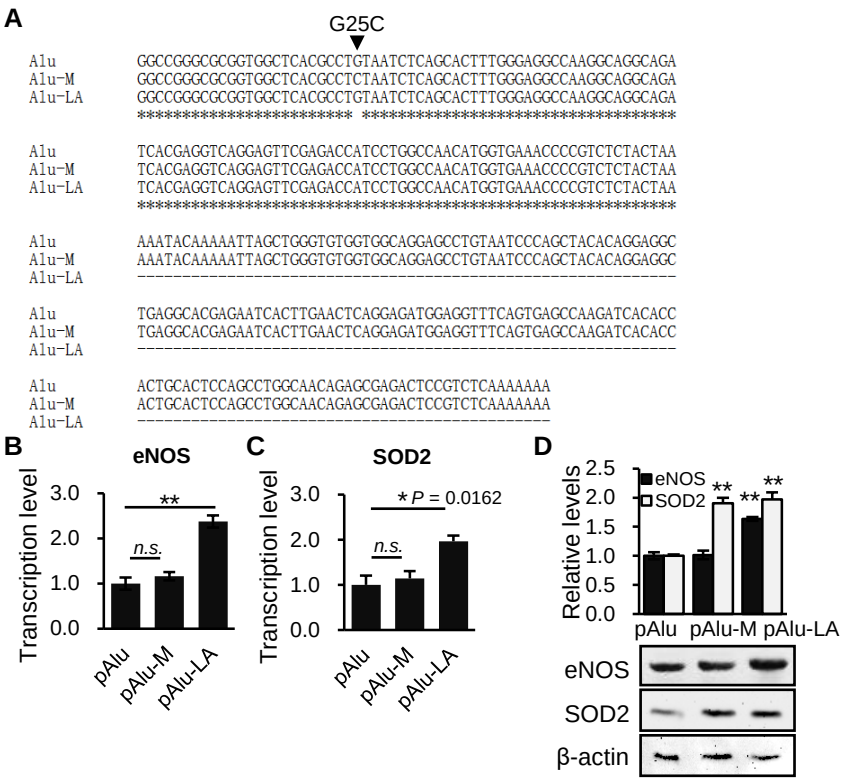
A
G25C
Alu GGCCGGGCGCGGTGGCTCACGCCTGTAATCTCAGCACTTTGGGAGGCCAAGGCAGGCAGA
Alu-M GGCCGGGCGCGGTGGCTCACGCCTCTAATCTCAGCACTTTGGGAGGCCAAGGCAGGCAGA
Alu-LA GGCCGGGCGCGGTGGCTCACGCCTGTAATCTCAGCACTTTGGGAGGCCAAGGCAGGCAGA
Alu TCACGAGGTCAGGAGTTCGAGACCATCCTGGCCAACATGGTGAAACCCCGTCTCTACTAA
Alu-M TCACGAGGTCAGGAGTTCGAGACCATCCTGGCCAACATGGTGAAACCCCGTCTCTACTAA
Alu-LA TCACGAGGTCAGGAGTTCGAGACCATCCTGGCCAACATGGTGAAACCCCGTCTCTACTAA
Alu AAATACAAAAATTAGCTGGGTGTGGTGGCAGGAGCCTGTAATCCCAGCTACACAGGAGGC
Alu-M AAATACAAAAATTAGCTGGGTGTGGTGGCAGGAGCCTGTAATCCCAGCTACACAGGAGGC
Alu-LA
Alu TGAGGCACGAGAATCACTTGAACTCAGGAGATGGAGGTTTCAGTGAGCCAAGATCACACC
Alu-M TGAGGCACGAGAATCACTTGAACTCAGGAGATGGAGGTTTCAGTGAGCCAAGATCACACC
Alu-LA
Alu ACTGCACTCCAGCCTGGCAACAGAGCGAGACTCCGTCTCAAAAAAA
Alu-M ACTGCACTCCAGCCTGGCAACAGAGCGAGACTCCGTCTCAAAAAAA
Alu-LA
B
eNOS
Transcription level
3.0
2.0
1.0
0.0
**
n.s.
pAlu
pAlu-M
pAlu-LA
C
SOD2
Transcription level
3.0
2.0
1.0
0.0
* P = 0.0162
n.s.
pAlu
pAlu-M
pAlu-LA
D
Relative levels
2.5
2.0
1.5
1.0
0.5
0.0
eNOS
SOD2
**
**
**
pAlu
pAlu-M
pAlu-LA
eNOS
SOD2
β-actin

Figure S1

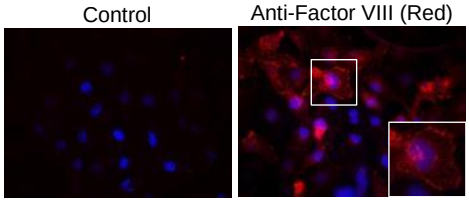

Figure S3

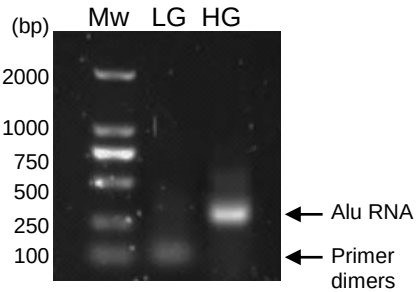

Figure S4

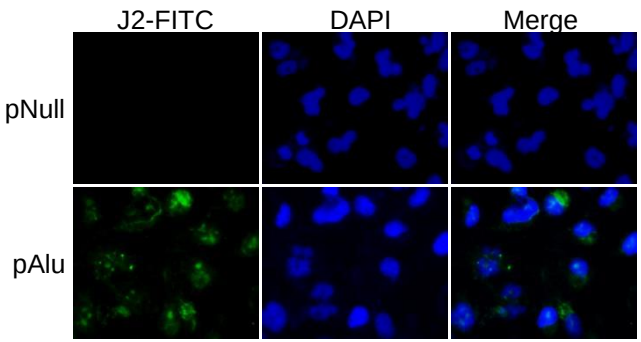

Figure S2

cDNA Library Sequencing and Classification

Homologous to	Counts	Samples
Alu Sc	23	S3, S4, S5, S14, S15, S17, S19, S22, S24, S27, S31, S32, S34, S37, S38, S39, S40, S41, S42, S43, S52, S55, S57
Alu Sx	4	S7, S10, S53, S58
Alu Sb	3	S2, S12, S35
Alu J	1	S6

Samples and sequences that were homologous to *Alu*-Sc subfamily:

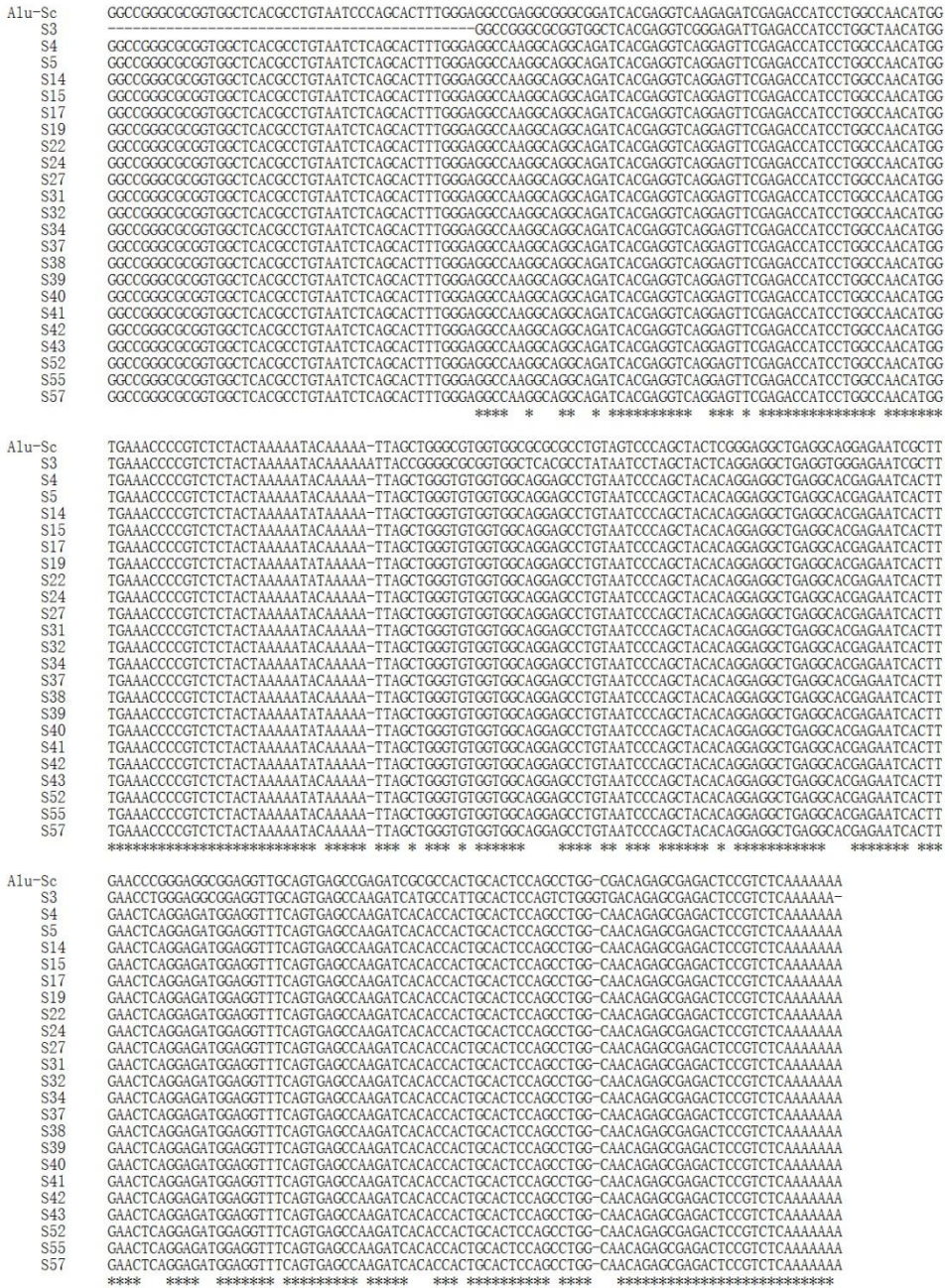

Samples and sequences that were homologous to *Alu*-Sx subfamily:

```
Alu-Sx      GGGCGGAGGCCGGGCGCGGTGGCTCACGCCTGTAATCCCAGCACTTTGGGAGGAAGATCACCTGAGGTCAGGAGTTCGAGAC
   S7       ------------GGGATCCT--CTAGAGATTCTACTCGGGAGGCTGAGGCGGGCAGATCACTTGAGGTCAGGAGTTGGAGAC
   S10      ----------------------------------ACTCGGGAGGCTGAGGCAGGTGGATCACTTGAGGTCAGGAGTTTGAGAC
   S53      GCTCGGTACCCGGGGATCCT--CTAGAGATTCTACTCGGGAGGCTGAGGCGGGCAGATCACTTGAGGTCAGGAGTTGGAGAC
   S58      --------------------T--CTAGAGATTCTACTCGGGAGGCTGAGGCGGGCAGATCACTTGAGGTCAGGAGTTGGAGAC
                                          * **      **  **  **  ****** ************** *****


Alu-Sx      CAGCCTGGCCAACATGGTGAAACCCCGTCTCTACTAAAAATACAAAAATTAGCCGGGCGTGGTGGCGCGCGCCTGTAATCCC
   S7       CAGCCTGGCCAACATAGTGAAACCCCGTCTCTACTAAAAATACAAAAGTTAGCCAGGTGTGGTG-----CATTTATA-----
   S10      CAGCCTGGCCAACATAGTGAAACCCCGTCTCTAATCGTCGACCTGCAGGCATGCAAGCTTGGCAC----TGGCCGTCGTTTT
   S53      CAGCCTGGCCAACATAGTGAAACCCCGTCTCTACTAAAAATACAAAAGTTAGCCAGGTGTGGTG-----CATTTATAATGGT
   S58      CAGCCTGGCCAACATAGTGAAACCCCGTCTCTACTAAAAATACAAAAGTTAGCCAGGTGTGGTG-----CATTTATAATG--
            *************** ***************** *       *   *   *  *  *  ***            *


Alu-Sx      AGCTACTCGGGAGGCTGAGGCAGGAGAATCGCTTGAACCCGGGAGGCGGAGGTTGCAGTGAGCCGAGATCGCGCCA
   S7       ---------------------------------------------------------------------------
   S10      ACAACGTCGTGA--CTGGGAAAACCCTGGCGTT---ACCCAACTTAATCGCCTTGCAGCACATCCCCCTTTCGCCA
   S53      TGGTGCCAGCT-------------------------------------------------------------------
   S58      ---------------------------------------------------------------------------
```

Samples and sequences that were homologous to *Alu*-Sb subfamily:

```
Alu-Sb      GGCCGGGCGCGGTGGCTCACGCCTGTAATCCCAGCACTTTGGGAGGCCGAGGCGGGCGGATCACGAGGTCAGGAGATCGA
   S4       GGCCGGGCGCGGTGGCTCACGCCTGTAATCTCAGCACTTTGGGAGGCCAAGGCAGGCAGATCACGAGGTCAGGAGTTCGA
   S12      GGCCGGGCGCGGTGGCTCACGCCTGTAATCCCAGCACTTTGGGAGGCCGAGGCGGGTGAATCATGAGGTCAGGAGATCGA
   S35      GGCCGGGCGCGGTGGCTCACGCCTGTAATCCCAGCACTTTGGGAGGCCGAGGCGGGTGAATCATGAGGTCAGGAGATCGA
            ****************************** ***************** **** **   **** *********** ****


Alu-Sb      GACCATCCTGGCTAACACGGTGAAACCCCGTCTCTACTAAAAATAC--A-----AAAATTAGCCGGGCGTGGTGGCGGGC
   S4       GACCATCCTGGCCAACATGGTGAAACCCCGTCTCTACTAAAAATAC------A-AAAATTAGCTGGGTGTGGTGGCAGGA
   S12      GACCATCCTGGCTAACAAGGTGAAACCCCGTCTCTACTAAAAATACAGAAAAAAAAAATTAGCCGGGCGCGAGGGCGGGC
   S35      GACCATCCTGGCTAACAAGGTGAAACCCCGTCTCTACTAAAAATACAGAAAAAAAAAATTAGCCGGGCGCGAGGGCGGGC
            ************ **** ****************************        ********* *** * *  *** **


Alu-Sb      GCCTGTAGTCCCAGCTACTCGGGAGGCTGAGGCAGGAGAATGGCGTGAACCCGGGAGGCGGAGCTTGCAGTGAGCCGAGA
   S4       GCCTGTAATCCCAGCTACACAGGAGGCTGAGGCACGAGAATCACTTGAACTCAGGAGATGGAGGTTTCAGTGAGCCAAGA
   S12      GCCTGTAGTCCCAGCTACTCGGGAGGCTGAGGCAGGAGAATGGCGTGAACCCGGGAAGCGGAGCTTGCAGTGAGCCGAGA
   S35      GCCTGTAGTCCCAGCTACTCGGGAGGCTGAGGCAGGAGAATGGCGTGAACCCGGGAAGCGGAGCTTGCAGTGAGCCGAGA
            ******* ********** * ************ ******  * ***** * ***   **** ** ********* ***


Alu-Sb      TCGCGCCACTGCACT-------CCAGCCTGGGCGACAGAGCGAGACTCCGTCTCAAAAAAAA
   S4       TCACACCACTGCACT-------CCAGCCTGG-CAACAGAGCGAGACTCCGTCTCAAAAAAA-
   S12      TTGCGTCACTGCAGTCCGCAGTCCGGCCTGGGTGACAGAGCGAGACTCCGTCTCAAAAAAAT
   S35      TTGCGTCACTGCAGTCCGCAGTCCGGCCTGGGTGACAGAGCGAGACTCCGTCTCAAAAAAAT
            *  *  ******* *       ** ******   ***************************
```

Samples and sequences that were homologous to *Alu*-J subfamily:

```
Alu-J       GGCCGGGCGCGGTGGCTCACGCCTGTAATCCCAGCACTTT----GGGAGGCCGAGGCGGGAGGATCACTTGAGCC
   S6       GGCCAGTGCCAAGCTTGCATGCCTGCAGGTCGACGATTCTACTCGGGAGGCTGAGGCAGGCCGATCAC--GAGGT
            **** *   *       ** ***** *   * *  * * *    ******* ***** **  ******  ***


Alu-J       CAGGAGTTCGAGACCAGCCTGGGCAACATAGTGAAACCCCGTCTCTACAAAAAATACAAAAATTAGCCGGGCGTG
   S6       CAGGAGTTCAAGATCAGCCTGGGCAACATAGTGAAACCCCGTCTAT-----AATCTCTAGAGGATCCCCGG-----
            ********* *** ******************************** *    **  *  * *   *  ****
```

Highlights

- Hyperglycemia leads to dsRNA accumulation in vascular endothelial cells.
- A pro-inflammatory and pro-oxidant mechanism for *Alu* RNA is proposed.
- *Alu* RNA negatively regulates eNOS and SOD2 at transcription and translation levels.